Noname manuscript No.
(will be inserted by the editor)

SWARM of UAVs based on FSO System using Differential Chaos Shift Keying

Ayesha Shahanaz Mohammad · Kavya Erla · Naga Sravani Muttanapalli · K Kesava · Anand Dharapu

Received: date / Accepted: date

Abstract A novel method is presented to analyse the effect of hovering-based Inter UAV-based FSO systems on the performance of serial-relaying DCSK. This study is more comprehensive than previous ones since the end-to-end BER analysis is done with the serial relaying DCSK. We analysed the end-to-end performance by considering hovering state positions, orientations, angle of arrival fluctuations, path loss, pointing loss and turbulence effect consideration. The atmospheric turbulence effect, hovering state fluctuations, and pointing error effect are mitigated using serial relay and DCSK techniques. This can improve the overall transmission distance of Inter UAV-based FSO systems by mitigating atmospheric turbulence and hovering state fluctuations. We derived the analytical BER expression for end-to-end serial relays by considering the DCSK. Derived analytical results are plotted and compared with the simulation results. This study gives Inter UAV-based FSO system design, serial relay performance under different turbulence, the required number of relays under specific turbulence conditions, and transmission distance.

Kavya Erla
Electronics and Communication Engineering, Dhanekula Institute of Engineering and Technology, Vijayawada, Gangur, Andhra Pradesh - 521139
Tel.: +919398467746
E-mail: kavyaerla770@gmail.com

Naga Sravani Muttanapalli
Electronics and Communication Engineering, Dhanekula Institute of Engineering and Technology, Vijayawada, Gangur, Andhra Pradesh - 521139
Tel.:+919392049303
E-mail: sravanimuthanapalli@gmail.com

Kanuri Kesava V V S N Murthy
Electronics and Communication Engineering, Dhanekula Institute of Engineering and Technology, Vijayawada, Gangur, Andhra Pradesh - 521139
Tel.: +919132862777
E-mail: keshukanuri0240@gamil.com

Anand Dharapu
Electronics and Communication Engineering, Dhanekula Institute of Engineering and Technology, Vijayawada, Gangur, Andhra Pradesh - 521139
Tel.: +919391139699
E-mail: ananddharapu1@gmail.com

I. INTRODUCTION

The demand for secure high-data-rate communication networks has grown innumerable times over the recent years due to the rise of wireless devices and the ever-growing demand for data-hungry applications. The benefits of Free Space Optical (FSO) communication, such as its high data rate, high bandwidth, and secure transmission, have made the technology promising. FSO system flexibility and applicability are further supplemented by the fact that they can be operated with Unmanned Aerial Vehicles (UAVs) that provide seamless means of accessing communication channels where disaster has hit: army, navy, civilian, and remote areas. One of the primary problems with FSO communication systems is that atmospheric turbulence, weather conditions, and pointing errors will cause the signal to deteriorate and generate higher error rates. In order to improve the overall system performance, Differential Chaos Shift Keying (DCSK) modulation has been employed as an alternative to mitigate the effects. In this paper, we proposed the DCSK modulation for the serial relay UAV-based FSO system to improve the link availability and high data rate, Extend the communication range and mitigate the turbulence effect; DCSK takes advantage of the characteristics of chaotic signals to offer improved performance in poor channel conditions. The work uses

the Gamma-Gamma model of turbulence to analyze the impacts of different system parameters. The results help design and optimize robust FSO communication links for UAV-based systems and promote the evolution of next-generation wireless communication technology.

The integration of UAV with FSO has been proposed in several studies [],[], []. There are three links in UAV-based FSO systems: Ground-to-UAV, UAV Ground, and UAV-to-UAV. The demand for UAV-to-UAV is very high in several applications such as last-mile access, disaster management, navy, maritime, and army. Several papers have investigated the importance of the Serial relay Inter UAV-based FSO system and its application with buffer-added relay technology proposed in the []. Serial relay inter UAV-based FSO systems are mainly affected by bad weather conditions. The system's performance under sand storm conditions was analyzed in the [].

The basic modelling and framework of UAV-based FSO were proposed for aerial-to-aerial, Ground-to-aerial, and aerial-to-ground and its challenges, such as noise floor, spectrum crowdedness, and security and a planer array for large field-of-view angels performance are investigated in [4]. The same author proposed that the spherical receiver for UAVs and optical mobile communication nodes were studied in [3]. [1], The paper outlines a vertical backhaul/fronthaul architecture design for 5G+ wireless systems based on UAVs and FSOs. It identifies weather-dependent link margins and data rates and indicates potential future deployment modes such as adaptive algorithms and hybrid FSO/RF solutions[1]. open-loop alignment/stability analysis of hovering multirotors and that rotational misalignment has more effect on performance than translational misalignment this analysis is studied in [5]. The basic modelling approach and framework for UAV-based FSO presented its applications between aerial-to-aerial, Ground-to-aerial, and aerial-to-ground systems while evaluating challenges regarding noise floor, spectrum crowdedness, and security and developed planer array solutions for field-of-view angle performance as detailed in [4]. A spherical receiver for UAVs and optical mobile communication nodes was investigated by the same author in [3]. [1] provides details about the vertical backhaul/fronthaul architecture design for 5G+ wireless systems which use UAVs and FSOs. The study defines data rate variations that rely on weather conditions alongside prospective implementation approaches featuring adaptive algorithms and hybrid FSO/RF systems[1]. The hovering stability analysis of multi-rotors operates using open-loop methods and rotational errors affect system performance substantially more than directional errors. The paper in [5] examines multi-rotor UAV applications in various free-space optical communication links through a combination of numerical simulation and Monte Carlo analysis data [7]. The model presented in [7] develops a suitable analytical channel description that combines path effects with atmospheric turbulence together with pointing errors and UAV AOA variability and provides simulation data for comparison. Further developments focus on finding the ideal position of UAV-based FSO according to research in [8] to maximize link stability with considerations for mechanical structures, payload and wind speed. The investigation in [9] and [8] explores UAV-based FSO as a relay using AF protocol while analyzing parameters, including orientation fluctuations alongside UAV position, optical beam width, and turbulence strength. A more reliable, secure, and power-efficient method using the MRR UAV-based FSO systems for Ground-to-UAV links was proposed in [10]. In [11], ground-to-UAV systems' ergodic capacity performance analysis was conducted [12]. Performance Analysis of ground-to-UAV systems under weak turbulence conditions can be found in the [13]. A performance evaluation of UAV-based FSO systems operating under different weather scenarios is presented within the research [18]. A study about POLSK modulation's Turbulence mitigation capabilities was presented in [19]. The model presents a new pointing error concept for UAV-based FSO systems while a comprehensive study exists in [21]. A Hybrid RF/FSO-assisted UAV system represents the innovative concept presented in [22].

A . Major contributions

This study examines the end-to-end performance of a serial relay UAV-based Free Space Optics (FSO) system utilizing Differential Chaos Shift Keying (DCSK) modulation. Several factors can degrade the performance of serial relay inter-UAV systems. DCSK modulation is remarkably robust against atmospheric turbulence and UAV fluctuations. This enhances the receiver's signal-to-noise ratio (SNR) at the UAV, which we investigate in this paper. This improves the larger communication range and the possible link availability with UAV-based FSO systems, which are crucial for UAV-based FSO systems, especially for cutting-edge applications and next-generation wireless networks. We discuss the performance of these systems concerning high data rates and secure communications. In our analysis, we propose DCSK modulation as a means to mitigate the effects of UAV fluctuations and atmospheric turbulence in unstable serial relay inter-UAV FSO systems. We also assess the end-to-end performance of the serial relay inter-UAV FSO system using DCSK modulation. For our performance evaluation, we consider

channels with moderate to strong turbulence modelled by the Gamma-Gamma distribution. Our findings indicate that the end-to-end average bit error rate of the serial relay inter-UAV FSO system is significantly improved by employing DCSK modulation combined with decode-and-forward transmission. The simulation results obtained from Monte Carlo simulations align well with those derived from closed-form expressions.

C. Organization

This paper analyzes the end-to-end performance of a serial relay inter-UAV Free Space Optics (FSO) system using Differential Chaos Shift Keying (DCSK) in conditions of moderate to strong turbulence. Sections II and III describe the serial relay inter-UAV FSO system and derive its analytical expression using the Meijer-G function. In Section IV, we derive expressions for the probability of error (P_e) in our proposed system utilizing DCSK modulation. Finally, Section V presents the numerical results for the serial relay inter-UAV FSO system with DCSK modulation and the conclusion.

II. SYSTEM MODEL AND MAIN ASSUMPTIONS

The serial relay inter UAV-based FSO system uses the configuration presented in Fig.1, where the source UAV sends data signals directly to the destination through UAV relay nodes. A source UAV generates the chaotic signal x_i through its built-in chaos generator. Each incoming binary data point is represented by +1 or -1, using the value b_l. The transmitted signal s_i presents the following mathematical representation according to [17].

$$s_i = \begin{cases} x_i, & \text{for } i = 1, 2, \ldots, M \\ b_l x_{i-m}, & \text{for } i = M+1, M+2, \ldots, 2M \end{cases}$$

The transmitted signal occupies two equal time slots during a one-bit duration while delivering both the original signal in the first slot and its delayed form in the second slot. DSCK modulation technique sends chaotic and information-bearing signals during a single-bit duration. A spreading factor equals $2M$ in this framework. The received signal r_k passes through a correlator to generate a decision variable that produces the binary output. A threshold detector produces binary output through an evaluation of correlator output c_l

$$\tilde{b_l} = \begin{cases} +1, & \text{if } c_l > 0 \\ -1, & \text{if } c_l < 0 \end{cases}$$

A. Received Signal Model

This system utilises intensity modulation and direct detection, with M-ary Pulse Position Modulation (PPM) as the modulation scheme. For simplicity, we denote the source node as node 0, which remains in a fixed position. The Unmanned Aerial Vehicles (UAVs), acting as relay nodes while hovering, are labelled as nodes 1, 2, ..., N. The destination node is referred to as node N+1. The system comprises N+1 links; each link i connects node i-1 to node i. Mathematically, the received electrical signal at node i in the ith link is defined as follows:

$$y_i = R h_i x_i + n_i, \quad i = 1, \cdots, N+1 \tag{1}$$

In this context, let R denote the responsivity of the photodetector (PD) at node i. The transmitted optical signal from node i is represented as x_i, while h_i denotes the channel coefficient of the i^{th} link. The signal-independent additive white Gaussian noise at this node is referred to as n_i. We assume that background noise is dominant at both the i^{th} relay and destination UAV, with a variance given by: $\sigma^2_{n,i} = 2q_e B_e R_{PD} P_b$ where q_e is the electron charge and B_e is the electrical bandwidth in Hz. The background power, denoted as P_b, is expressed as: $P_b = B_0 A_a N_b(\lambda) \Omega_{FOV,i}$ Here, B_0 is the optical filter bandwidth (in µm), A_a is the lens area (in cm^2), and $N_b(\lambda)$ represents the spectral radiance of background radiation at a specific wavelength λ (in Watts per ($\text{cm}^2 \cdot \mu\text{m} \cdot \text{sr}$)). The receiver FOV of the i^{th} relay, in steradians, is denoted as $\Omega_{FOV,i}$, calculated as: $\Omega_{FOV,i} \simeq \pi \theta^2_{FOV,i}$ Here, $\theta_{FOV,i}$ is the FOV angle in mrad. The instantaneous SNR at the i^{th} receiver UAV is defined as: $\gamma_i = \frac{P_t^2 R_{PD}^2 h_i^2}{\sigma^2_{n,i}}$ In this equation, P represents the average transmitted power, which is linked with the total transmit power P_t. Assuming multiple hops via UAVs between the source and destination, [18].

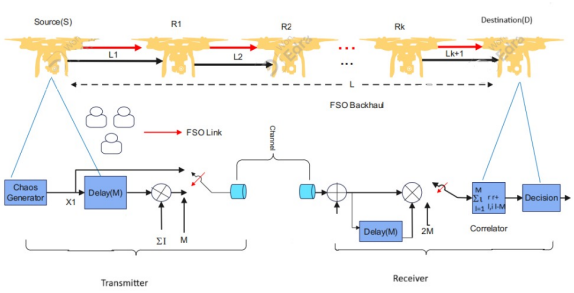

Fig. 1: The conceptual framework of a serial relay UAV-based FSO communication system utilizing DCSK modulation with a DF protocol.

III. CHANNEL MODEL

This system includes UAV-to-UAV communication links. A system starts with a Source link followed by UAV-UAV links before reaching its final Destination link. The UU links exist between the second and N links that come after the initial and before the $(N+1)$-th link. The total channel gain h_i for each of these links can be expressed as the product of four different impairments:

$$h_i = h_i^{(a1)} \cdot h_i^{(\mathrm{aa})} \cdot h_i^{(\mathrm{pe})} \cdot h_i^{(\mathrm{aoa})}, \quad i = 1, \ldots, N+1$$

In this equation, $h_i^{(a1)}$ represents atmospheric loss, $h_i^{(\mathrm{aa})}$ accounts for atmospheric turbulence, $h_i^{(\mathrm{pe})}$ pertains to pointing error, and $h_i^{(\mathrm{aoa})}$ reflects link interruptions caused by fluctuations in the angle of arrival (AoA). Our analysis offers performance-enhancing larger distance coverage, improving the link distance and mitigating the UAV fluctuations. For each link based on the principles described in references [17], [18] and [25]. All other parameters in the $N+1$ links stay constant unless additional indicating conditions are provided.

3.1 Atmospheric attenuation

The air medium reduces Signals during transmission due to absorption and scattering phenomena. The atmospheric concentration of substance, which causes signal attenuation, fluctuates spatially and temporally and is affected by atmospheric conditions. The reduction of optical power as it traverses the atmosphere is characterized by the exponential Beer-Lambert equation, articulated as follows:

$$h_i^{a1} = \exp\left(-\alpha_p Z_i\right) \tag{2}$$

In this equation, α_p denotes the attenuation coefficient, whereas Z_i signifies the transmission distance for the i-th hop.

3.2 Atmospheric turbulence

The popular turbulence model depicts atmospheric changes as distinct air cells or eddies, characterized by varying sizes and refractive indices. In geometrical optics, these eddies function as lenses that randomly refract the optical wavefront, leading to a distorted intensity profile at the receiver of a communication system. The variation in intensity, referred to as scintillation, is a significant element that restricts the efficiency of an atmospheric FSO communication link. This research will examine system performance in a moderate to strong turbulence regime. We shall employ the Gamma-Gamma distribution to characterize the atmospheric turbulence channel. The probability distribution function (PDF) of the intensity fluctuation (h_i^{aa}) induced by air turbulence is thus represented by [21]

$$f_{h_i^{\mathrm{aa}}}\left(h_i^{\mathrm{aa}}\right) = \frac{2\left(\alpha_i\beta_i\right)^{(\alpha_i+\beta_i)/2}}{\Gamma\left(\alpha_i\right)\Gamma\left(\beta_i\right)} \left(h_i^{\mathrm{aa}}\right)^{\frac{\alpha_i+\beta_i}{2}-1} K_{\alpha_i-\beta_i}\left(2\sqrt{ha_i\beta_i h_i^{\mathrm{aa}}}\right), \quad h_i^{\mathrm{aa}} > 0 \tag{3}$$

Here, $\Gamma(\cdot)$ represents the Gamma function, and $K_{\alpha_i-\beta_i}(\cdot)$ signifies the modified Bessel function of the second kind of order $\alpha_i - \beta_i$. In this context, α_i and β_i denote the relative quantities of small-scale and large-scale eddies present in the scattering environment.

They are written as [21]

$$\alpha_i = \left[\exp\left(\frac{0.49\sigma_{\mathrm{R},i}^2}{\left(1+1.11\sigma_{\mathrm{R},i}^{12/5}\right)^{7/6}}\right) - 1\right]^{-1}$$

$$\beta_i = \left[\exp\left(\frac{0.51\sigma_{\mathrm{R}}^2}{\left(1+0.69\sigma_{\mathrm{R},i}^{12/5}\right)^{5/6}}\right) - 1\right]^{-1}$$

where, $\sigma_{\mathrm{R},i}^2 = 1.23C_n^2k^{7/6}Z_i^{11/6}$ represents the Rytov variance associated with the link distance. Z_i, C_n^2 represents the index of refraction structure parameter of the atmosphere, whereas $k = 2\pi/\lambda$ denotes the optical wave number, with λ indicating the wavelength.

3.3 Misalignment fading models

A significant challenge in UAV-FSO systems is the pointing error, which can occur due to the UAV's position or orientation, in addition to external influences such as wind and turbulence. These flaws can substantially impair the system's performance. At both ends of the receiver, a circular detecting aperture with a radius r_a is positioned at node i, where $i = 1, \ldots, N+1$. The radial displacement vector from the center of the receiving aperture to the beam center is represented as $\mathbf{r}_{\mathrm{d},i} = [x_{\mathrm{d},i}, y_{\mathrm{d},i}]$. Three things affect the received optical signal:

1. fluctuations in the orientations of the transmitters are represented as $\mathbf{r}_{\theta_{\mathrm{t}},i} = [x_{\theta_{\mathrm{t}},i}, y_{\theta_{\mathrm{t}},i}]$.

2. fluctuations in the transmitter positions, represented as $\mathbf{r}_{\mathrm{t},i} = [x_{\mathrm{t},i}, y_{\mathrm{t},i}]$.

3. fluctuations in the positions of the receivers, represented as $\mathbf{r}_{\mathrm{r},i} = [x_{\mathrm{r},i}, y_{\mathrm{r},i}]$.

At the receiver, these variations are Gaussian distributed represented along the vertical and horizontal axes and are represented as follows [18]:

$$\begin{cases} x_{\mathrm{d},i} = x_{\mathrm{t},i} + x_{\mathrm{r},i} + x_{\theta_{\mathrm{t}},i} \\ y_{\mathrm{d},i} = y_{\mathrm{t},i} + y_{\mathrm{r},i} + y_{\theta_{\mathrm{t}},i} \end{cases} \tag{4}$$

The end-to-end serial relay UAV-based FSO system consists of three distinct links, which are classified as follows:

a) $UAV - to - UAV$ links: both Both the transmitter and receiver are positioned at $x_{\mathrm{t},i}$ and $x_{\mathrm{r},i}$, which follow a Gaussian distribution. Specifically, $x_{\mathrm{t},i}, x_{\mathrm{r},i} \sim \mathcal{N}\left(0, \sigma^2_{\mathrm{p,uu}}\right)$. Additionally, we have $x_{\theta_{\mathrm{t}},i} \approx Z_i \theta_{\mathrm{tx},i}$, where $\theta_{\mathrm{tx},i} \sim \mathcal{N}\left(0, \sigma^2_{\mathrm{angle,uu}}\right)$.

This implies that $x_{\theta_{\mathrm{t}},i} \sim \mathcal{N}\left(0, Z_i^2 \sigma^2_{\mathrm{angle,uu}}\right)$.

Similarly, we can analyze the distribution of $y_{\mathrm{d},i}$. As a result, both $x_{\mathrm{d},i}$ and $y_{\mathrm{d},i}$ are distributed as

$\mathcal{N}\left(0, 2\sigma^2_{\mathrm{p,uu}} + Z_i^2 \sigma^2_{\mathrm{angle,uu}}\right)$.

The total fluctuation can lead to the pointing error at i^{th} link , which is Rayleigh distribution defined as follows $r_{\mathrm{tr},i} = \sqrt{x^2_{\mathrm{d},i} + y^2_{\mathrm{d},i}}$

$$f_{r_{\mathrm{tr},i}}\left(r_{\mathrm{tr},i}\right) = \frac{r_{\mathrm{tr},i}}{\sigma^2_{\mathrm{t},i}} \exp\left(-\frac{r^2_{\mathrm{tr},i}}{2\sigma^2_{\mathrm{t},i}}\right), \quad r_{\mathrm{tr},i} \geq 0 \tag{5}$$

The pointing loss varies among different links. The variance $\sigma^2_{\mathrm{t},i}$ for various links is defined as follows:

$$\sigma^2_{\mathrm{t},i} = \left\{\sigma^2_{\mathrm{p,uu}} + \sigma^2_{\mathrm{p,\ gu}} + Z^2_{N+1}\sigma^2_{\mathrm{angle\ ,uu}}, \quad i = N+1\right.$$

The Probability Density Function (PDF) of the pointing error $h_i^{(\mathrm{pe})}$ is defined as follows [20],

$$f_{h_i^{(\mathrm{pe})}}\left(h_i^{(\mathrm{pe})}\right) = \frac{\gamma_i^2}{A_i^{\gamma_i^2}}\left(h_i^{(\mathrm{pe})}\right)^{\gamma_i^2 - 1} \quad 0 \leq h_i^{(\mathrm{pe})} \leq A_i, \quad i = 1, \cdots, N+1 \tag{6}$$

Where $A_i = [\mathrm{erf}(v_i)]^2$ represents the fraction of the collected power at i receiver. where $v_i = \frac{\sqrt{\pi} r_a}{\sqrt{2} w_{z,i}}$ Additionally, $\gamma_i^2 = \frac{w^2_{zeq}}{i \cdot 4\sigma^2_{\mathrm{s},i}}$ The quantity $\omega^2_{z_{\mathrm{eq},i}}$, which is defined as $\omega^2_{z,i}\sqrt{\frac{\pi}{2}} \cdot \frac{\mathrm{erf}(v_i)}{2 v_i e^{-v_i^2}}$, approximates to $\omega^2_{z,i} + \frac{3}{2\sqrt{2}}$ and represents the equivalent beam width [30].

3.4 Overall Channel Statistical Characteristic

Where the channel state consists of four states, three are independent random variables, and the remaining one is deterministic. With these assumptions, the PDF is expressed as follows.

$$h_i = h_i^{(1)} h_i^{(\mathrm{a})} h_i^{(\mathrm{pe})} h_i^{(\mathrm{aoa})}, \tag{7}$$

In this analysis, the channel state consists of four distinct states. Among these, three are independent random variables, while the fourth is deterministic. Based on these assumptions, the probability density function (PDF) can be expressed as follows. For the sake of simplicity, we assume that h_{ii} represents the combined PDF of $h_i^{(1)}$, $h_i^{(a)}$, and $h_i^{(pe)}$.

This h_{ii} can be mathematically represented as follows [18]

$$f_{h_{ii}}\left(h_{ii}\right) = \int f_{h_{ii}|h^{\mathrm{a}}_{ii}}\left(h_{ii} \mid h_i^{\mathrm{a}}\right) f_{h_i^{\mathrm{a}}}\left(h_i^{\mathrm{a}}\right) \mathrm{d}h_i \tag{8}$$

where $f_{h_{ii}|h_i^a}\left(h_{ii} \mid h_i^{\mathrm{a}}\right)$, which is presented more detail in [18], is the condition probability given h_i^{a}. As $f_{h_i^{\mathrm{a}}}$ is Gamma Gamma distribution, $f_{h_{ii}}\left(h_{ii}\right)$ is given by [18]

$$f_{h_{ii}}\left(h_{ii}\right) = \frac{2\gamma_i^2 \left(\alpha_i \beta_i\right)^{(\alpha_i+\beta_i)/2}}{\left(A_{0,i} h_i^1\right)^{\gamma_i^2} \Gamma\left(\alpha_i\right) \Gamma\left(\beta_i\right)} h_{ii}^{\gamma_i^2 - 1} \int_{h_i/A_{0,i}h_i^1}^{\infty} \left(h_i^{\mathrm{a}}\right)^{(\alpha_i+\beta_i)/2-1-\gamma_i^2} K_{\alpha_i-\beta_i}\left(2\sqrt{\alpha_i\beta_i h_i^{\mathrm{a}}}\right) \mathrm{d}h_i^{\mathrm{a}} \tag{9}$$

By utilizing the equations [23, Eq. (9.34.3)] and [24, Eq. (07.34.21.0085.01)], a closed-form expression in terms of Meijer's G functions is obtained as follows:

$f_{h_{ii}}\left(h_{ii}\right) = \frac{\alpha_i \beta_i \gamma_i^2}{A_{0,i} h_i^{\Gamma} \Gamma(\alpha_i) \Gamma(\beta_i)} \left(\frac{\alpha_i \beta_i h_{ii}}{A_{0,i} h_i^l}\right)^{\frac{\alpha_i+\beta_i}{2}-1}$

$$\times G_{1,3}^{3,0}\left[\frac{\alpha_i\beta_i h_{ii}}{A_{0,i}h_i^1}\middle|\begin{matrix}1-\frac{\alpha_i+\beta_i}{2}+\gamma_i^2\\ -\frac{\alpha_i+\beta_i}{2}+\gamma_i^2,\frac{\alpha_i-\beta_i}{2},\frac{-\alpha_i+\beta_i}{2}\end{matrix}\right] \tag{10}$$

By further simplifying the above expression and using [24, Eq. (07.34.16.0001.01)], we can derive the final closed-form expression for $f_{h_i}(h_i)$.

$$f_{h_{ii}}(h_{ii}) = \frac{\alpha_i\beta_i\gamma_i^2}{A_{0,i}h_i^l\Gamma(\alpha_i)\Gamma(\beta_i)}$$

$$G_{1,3}^{3,0}\left[\frac{\alpha_i\beta_i}{A_{0,i}h_i^h}h_{ii}\middle|\begin{matrix}\gamma_i^2\\ \gamma_i^2-1,\alpha_i-1,\beta_i-1\end{matrix}\right] \tag{11}$$

(i.e., $\theta_{\mathrm{tx},i}$ and $\theta_{\mathrm{ty},i}$) contribute to the pointing error and the AoA fluctuation simultaneously, the correlation between $h_i^{(\mathrm{pe})}$ and $h_i^{(\mathrm{aoa})}$ is weak when $\theta_{\mathrm{FoV},i} \gg \sigma_{\mathrm{angle,\,u}}$. The reason is provided as follows. Note that $\sigma_{\mathrm{angle,}}$ is the standard deviation of $\theta_{\mathrm{tx},i}$ and $\theta_{\mathrm{ty},i}$. Under a small value of $\sigma_{\mathrm{angle,u}}$ relative to $\theta_{\mathrm{FoV},i}$, compared with $\mathbf{r}_{\mathrm{t},i}$ and $\mathbf{r}_{\mathrm{r},i}$, the impact of $\mathbf{r}_{\theta_{\mathrm{t}},i} \simeq [Z_i\theta_{\mathrm{tx},i}, Z_i\theta_{\mathrm{ty},i}]$ in Fig. 2 on pointing error is weak. This indicates that the transmitter's orientation misalignment is weakly correlated with pointing error when $\theta_{\mathrm{FoV},i} \gg \sigma_{\mathrm{angle,}}$. Moreover, when $\theta_{\mathrm{FoV},i} \gg \sigma_{\mathrm{angle,u}}, \theta_{\mathrm{tx},i}$ and $\theta_{\mathrm{ty},i}$ have little effect on $\theta_{\mathrm{a},i}$, and thus the transmitter's orientation misalignment and the AoA fluctuation are also weakly correlated. Consequently, the four impairments in (3) can be approximated as independent variables. Specially, for the GU link, the pointing error and the AoA fluctuation are no longer relevant since orientation deviations of the source node are approximately zero, and these four impairments are practically independent.

According to the above analysis, the PDF of h_i is approximated as

$$f_{h_i}(h_i) \simeq \int_0^{+\infty} \frac{1}{h_{ii}} f_{h_i^{(\mathrm{aoa})}}\left(\frac{h_i}{h_{ii}}\right) f_{h_{ii}}(h_{ii})\,\mathrm{d}h_{ii} \tag{12}$$

where $h_{ii} \triangleq h_i^{(1)}h_i^{(a)}h_i^{(pe)}$. By resolving equation (15), we obtain the probability density function (PDF) of h_i, which is described in below.

For the serial relay UAV-based FSO M-ary pulse position modulation (PPM) system, the PDF of the overall channel gain h_i is approximated as

$$f_{h_i}(h_i) \simeq \exp\left(-\frac{\theta_{\mathrm{FoV},i}^2}{2m_i\sigma_{\mathrm{angle\ ,u}}^2}\right)\delta(h_i) + \left[1-\exp\left(-\frac{\theta_{\mathrm{FoV},i}^2}{2m_i\sigma_{\mathrm{angle\ ,u}}^2}\right)\right]\frac{\alpha_i\beta_i\gamma_i^2}{A_i h_i^1\Gamma(\alpha_i)\Gamma(\beta_i)} \times G_{1,3}^{3,0}\left(\begin{matrix}\gamma_i^2\\ \gamma_i^2-1,\alpha_i-1,\beta_i-1\end{matrix}\middle|\frac{\alpha_i\beta_i h_i}{(A_i h_i^1)}\right). \tag{13}$$

$$f_h(h) \approx a_1\delta(h) + f_h(h>0), \tag{14}$$

where, a_i is $\exp\left(-\frac{\theta_{\mathrm{FoV},i}^2}{2m_i\sigma_{\mathrm{angle\ ,u}}^2}\right)$ and
$f_h(h>0)$ is (1-a_i) $*$ $\frac{\alpha_i\beta_i\gamma_i^2}{A_i h_i^1\Gamma(\alpha_i)\Gamma(\beta_i)}$
$\times\, G_{1,3}^{3,0}\left(\begin{matrix}\gamma_i^2\\ \gamma_i^2-1,\alpha_i-1,\beta_i-1\end{matrix}\middle|\frac{\alpha_i\beta_i h_i}{(A_i h_i^1)}\right)$

IV. PERFORMANCE ANALYSIS

4.1. Calculation of Probability of Error

This paper presents the error rate of DCSK as characterized by instantaneous SNR per bit following [17].

$$P_e(h_i) = Q\sqrt{\frac{h_i}{2}\left(1+\frac{M}{2h_i}\right)^{-1}} \tag{15}$$

Eq. (8) represents the form of the statistical analysis when $Q(h_i) = (1/2)\,\mathrm{erfc}(h_i/\sqrt{2})$.

$$P_e(h_i) = \frac{1}{2}\,\mathrm{erfc}\sqrt{\frac{h_i}{4}\left(1+\frac{M}{2h_i}\right)^{-1}} \tag{16}$$

$$P_e = \int_0^{\infty} P_e(h_i)\, f_{\gamma_b}(h_i)\, dh_i \tag{17}$$

Using the expression $\mathrm{erfc}(\sqrt{z}) = \frac{1}{\sqrt{\pi}}G_{1,2}^{2,0}\left(z\middle|\begin{matrix}1\\ 0,\frac{1}{2}\end{matrix}\right)$

Putting the values of $f_{\gamma_b}(\gamma_b)$ and $P_e(\gamma_b)$ from (7) and (9) in (10), respectively, we get the following equation

$$P_e(h_i) \simeq \int_0^{\infty}\frac{1}{2}G_{1,2}^{2,0}\left(\frac{\gamma_b}{4}\left(1+\frac{M}{2\gamma_b}\right)^{-1}\middle|\begin{matrix}1\\ 0,\frac{1}{2}\end{matrix}\right)\times\exp\left(-\frac{\theta_{\mathrm{FoV},i}^2}{2m_i\sigma_{\mathrm{angle\ ,u}}^2}\right)\delta(h_i) + \left[1-\exp\left(-\frac{\theta_{\mathrm{FoV},i}^2}{2m_i\sigma_{\mathrm{angle\ ,u}}^2}\right)\right]\frac{\alpha_i\beta_i\zeta_i^2}{A_i h_i^1\Gamma(\alpha_i)\Gamma(\beta_i)}\times G_{1,3}^{3,0}\left(\begin{matrix}\gamma_i^2\\ \gamma_i^2-1,\alpha_i-1,\beta_i-1\end{matrix}\middle|\frac{\alpha_i\beta_i h_i}{(A_i h_i^1)}\right) \tag{18}$$

To solve the integral mentioned above, we can us the identity referenced in Equation [[32], Eq. (2.24.1.3 This approach yields the following result:

$$P_i \simeq \frac{a_i}{2} + \frac{1-a_i}{2} \frac{\alpha_i \beta_i \zeta_i^2}{A_i h_i^1 \Gamma(\alpha_i)\Gamma(\beta_i)} \sum_{n=0}^{\infty} \frac{(1/4 - M/8)^n}{n!} \times G_{4,5}^{3,3}\left(\begin{matrix} \gamma_i^2, 0, n, 1/2 \\ \gamma_i^2 - 1, \alpha_i - 1, \beta_i - 1, n-1, n \end{matrix} \middle| \frac{\alpha_i \beta_i}{A_i h_i^1} \right) \quad (19$$

The serial relay UAV-based free space optical (FSC system, consisting of $N+1$ hops (which include N re lays), can be modeled as a series of $N+1$ M-symmetric channels. Each hop has an associated error probability denoted as P_i for the ith hop (as illustrated in Fig. 2). Assuming that each hop is independent, the overall end-to-end symbol error probability, denoted as P_e, can be calculated as follows

$$P_{e2e} = 1 - \prod_{i=1}^{M+1} \left(1 - P_e(h_i)\right) \quad (20$$

Substitute equation (19) into equation (20) to obtai the simplified end-to-end bit error rate.

V Results and Discussions

A comparison of SNR and BER average values emerge from analyzing both analytical and simulated result for systems functioning under specific conditions. Results from the BER evaluation consider the varying M spread from 4 through 20 to 40 combined with two different values of σ_R^2 at 1.3 and 4. The system performance strengthens because higher signal quality produces lower BER which has been proven through these observations. The BER performance shows substantial improvement when the relay channel has low variance ($\sigma_R^2 = 1.3$) than when it has higher variance ($\sigma_R^2 = 4$) since reduced channel fading improves system reliability. The theoretical model accuracy for performance analysis can be verified because analytical curves match simulation results perfectly.

The graphic in the figure shows how average BER changes relative to average SNR variations when the user diversity equals $N = 4, 3, 2, 1$. The model accuracy receives verification through analysis of results which shows solid black lines indicating analytical results while red circles show simulation results. The communication system provides enhanced BER quality when N value rises particularly within the lower to moderate SNR ranges. Diversity operating in conjunction with cooperative gain results in better performance quality.

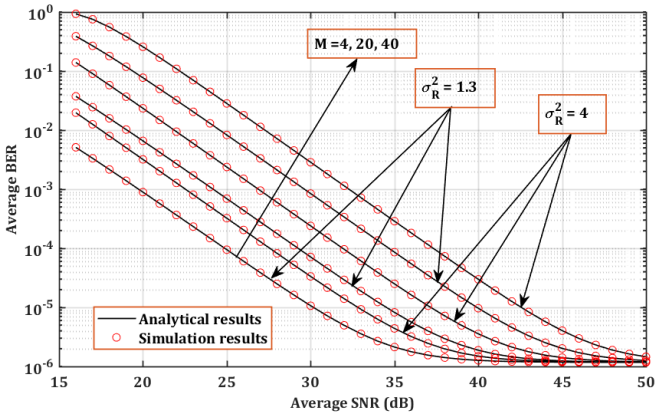

Fig. 2: Average BER of Inter UAV FSO Link versus average SNR over moderate to strong turbulence channel model for $\sigma_{to} = \sigma_{ro} = 3mrad, Z = 250m, \sigma_R = 10$.

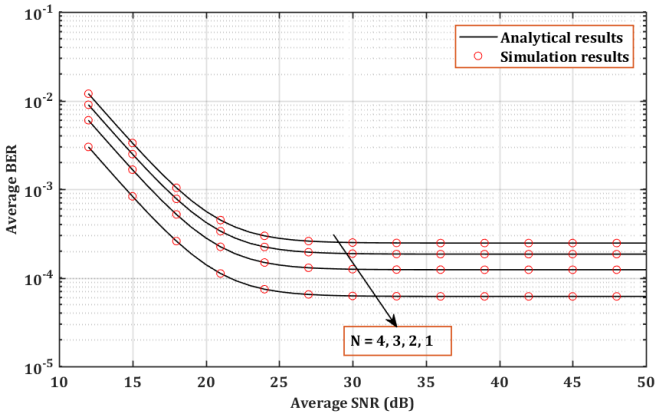

Fig. 3: Average BER of Inter UAV FSO Link versus average SNR over moderate to strong turbulence channel model for $\sigma_{to} = \sigma_{ro} = 3mrad, Z = 250m, \sigma_R = 10$. $\sigma_{to} = \sigma_{ro} = 4mrad, \sigma_{tp} = \sigma_{rp} = 3cm$.

The BER curves stay flat when the SNR reaches 30 dB since system limitations create an upper boundary that likely stems from noise interferences or propagation errors with unknown origins. Experimental findings match theoretical model results which demonstrates the theoretical models develop precise estimates of system reaction patterns.

The figure assesses the Bit Error Rate (BER) performance variability across different average Signal-to-Noise Ratio (SNR) levels at three through six mrad angular standard deviation $\sigma_{to} = \sigma_{ro} =$. A free-space optical or wireless optical communication system demonstrates these parameters as standard deviation measures for the pointing error between devices at the transmitter and receiver ends. The transmission reliability reduces because equipment points deviating from their

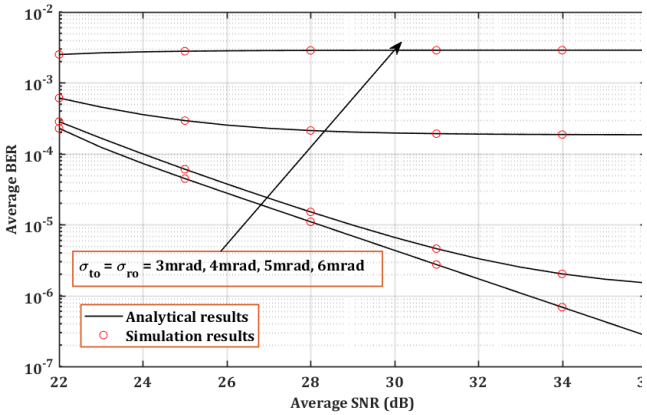

Fig. 4: PAverage BER of Inter UAV FSO Link versus average SNR over moderate to strong turbulence channel model for $\sigma_{to} = \sigma_{ro} = 3mrad, Z = 250m$, $\sigma_R = 10$. $\sigma_{to} = \sigma_{ro} = 4mrad$, $\sigma_{tp} = \sigma_{rp} = 3cm$.

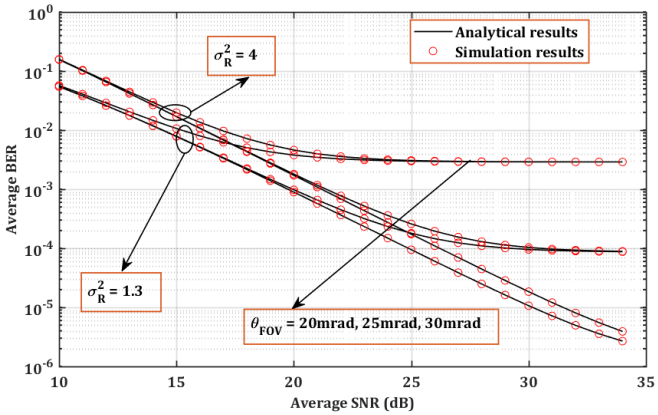

Fig. 5: P_{out} versus Average SNR for various values of C_n^2 with HD detection under maritime turbulence, and $\sigma_{to} = \sigma_{ro} = 4mrad$, θ_{FOV}, $L = 1000m$.

intended direction cause the performance results to show negative impacts. When point deviation stays below 3 mrad the system achieves better BER performance however the system creates an error threshold when this angle exceeds 6 mrad. The system shows extreme vulnerability to all errors in its directional orientation capabilities. The theoretic prediction model exhibits precise accuracy for realistic performance predictions because its analytical solids precisely match simulated outcomes (red circles).

To visually demonstrate the Bit Error Rate (BER) performance against Signal-to-Noise Ratio (SNR) averages the figure presents results from different relay channel variance values $\sigma_R^2 = 1.3$ and $\sigma_R^2 = 4$ while showing results from several Field of View (FOV) receiver angles $\theta_{\text{FOV}} = 20$ mrad, 25 mrad, and 30 mrad. A decreased relay channel variance produces substantial improvements in BER performance thus verifying better system reliability through reduced fading and interference in the relay link. The system performance enhances as the FOV angle grows larger because wider FOV helps the receiver handle angular misalignment resulting from pointing errors. The system performance reaches a point of saturation at elevated SNRs which establishes a BER floor attributed either to residual misalignment among other factors unrelated to SNR. Results obtained from analyzing mathematical models show strong accuracy by matching the simulation results with analytical curves (solid lines) and red circles.

This paper investigated the channel modelling, outage probability analysis, and parameter optimization for UAV-based FSO relaying systems. A tractable and accurate channel model was established by taking into account atmospheric loss, atmospheric turbulence, pointing error, and link interruption due to AoA fluctuation. Based on the channel
model, closed-form expressions were obtained for link outage probability and end-to-end outage probability. Subsequently, the asymptotic outage performance bounds were also investigated. Moreover, the beam width, FoV and UAVs' locations were optimized. Numerical results verify the accuracy of the derived theoretical expressions and the efficiency of the proposed optimization schemes. The obtained theoretical expressions enable designers to evaluate outage performance rapidly without time-intensive simulations. The derived parameter optimization results can help determine the optimal available parameter choices when designing the UAV-based FSO systems.

The figure exhibits how position variance ($\sigma_{tp} = \sigma_{rp}$) affects the average Bit Error Rate (BER) when compared to Signal-to-Noise Ratio (SNR) in a DCSK system. The figure presents BER curves that represent data points obtained from position changes of 4 cm, 5 cm, 6 cm, and 7 cm. The analytical results represented through solid lines match very closely with the simulation results using red circles which verifies the theoretical model. The measurement data showed BER reduction because SNR values increased thus leading to better transmission quality. A high amount of positional variance between σ_{tp} and σ_{rp} results in performance degradation of the BER system. The signal reception suffers degradation because position variations cause larger misalignments and beam spread. System reliability of DCSK-based communication improves when transmitter and receiver positions can be minimized for fluctuations.The figure exhibits how position variance ($\sigma_{tp} = \sigma_{rp}$) affects the average Bit Error Rate (BER) when compared to Signal-to-Noise Ratio (SNR) in a

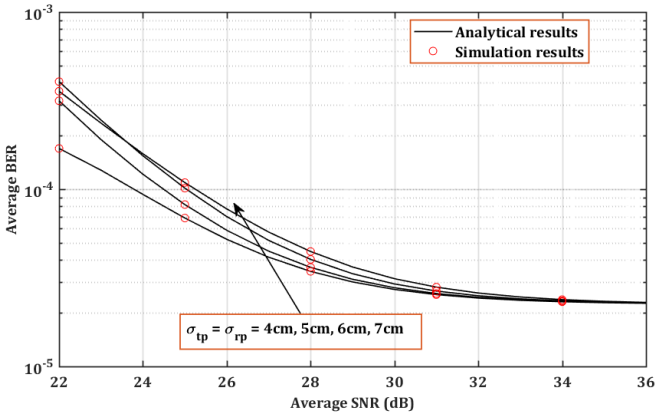

Fig. 6: Average BER of Inter UAV FSO Link versus average SNR over moderate to strong turbulence channel model for $\sigma_{to} = \sigma_{ro} = 3mrad, Z = 250m$, $\sigma_R = 10$. $\sigma_{to} = \sigma_{ro} = 3mrad, Z = 250m$, $\sigma_R = 10$. and $\sigma_{to} = \sigma_{ro} = 4mrad$, $\sigma_{tp} = \sigma_{rp} = 3cm$.

DCSK system. The figure presents BER curves that represent data points obtained from position changes of 4 cm, 5 cm, 6 cm, and 7 cm. The analytical results represented through solid lines match very closely with the simulation results using red circles which verifies the theoretical model. The measurement data showed BER reduction because SNR values increased thus leading to better transmission quality. A high amount of positional variance between σ_{tp} and σ_{rp} results in performance degradation of the BER system. The signal reception suffers degradation because position variations cause larger misalignments and beam spread. System reliability of DCSK-based communication improves when transmitter and receiver positions can be minimized for fluctuations.

VI Conclusion and Future Scope

This research examines the outage performance of the maritime inter-UAV-based free-space optical communication system. The performance is evaluated through HD detection, accounting for atmospheric turbulence, pointing error, fluctuations in the angle of attack of hovering UAVs, and attenuation. The findings indicate that maritime turbulence and pointing errors associated with the hovering state of UAVs are the primary factors that diminish the performance of inter-UAV-based free space optical communication systems. A lognormal distribution effectively models the maritime turbulent channel and is extensively studied. The outage probability is analyzed for various channel parameters, including W_Z, average SNR, θ_{FOV}, σ_{to}, σ_{ro}, and additional channel parameters. The results indicate that HD effectively compensates for the UAV's orientation deviations and mitigates the impact of maritime turbulence when compared to alternative detection techniques. The proposed system effectively enhances maritime communications by integrating UAVs to supplement shore- and satellite-based deployments, thereby offering an intermediate aerial layer that addresses the coverage limitations of terrestrial optical links and narrowband satellite links.

References

1. Alzenad, Mohamed, et al. "FSO-based vertical backhaul/fronthaul framework for 5G+ wireless networks." IEEE Communications Magazine 56.1 (2018): 218-224.
2. Majumdar, Arun K. Advanced free space optics (FSO): a systems approach. Vol. 186. Springer, 2014.
3. Kaadan, Asaad, Hazem Refai, and Peter Lopresti. "Spherical FSO receivers for UAV communication: geometric coverage models." IEEE Transactions on Aerospace and Electronic Systems 52.5 (2016): 2157-2167.
4. Kaadan, Asaad, et al. "Modeling of aerial-to-aerial short-distance free-space optical links." 2013 Integrated Communications, Navigation and Surveillance Conference (ICNS). IEEE, 2013.
5. Kaadan, Asaad, Hazem H. Refai, and Peter G. LoPresti. "Multielement FSO transceivers alignment for inter-UAV communications." Journal of Lightwave Technology 32.24 (2014): 4785-4795.
6. Dabiri, Mohammad Taghi, Seyed Mohammad Sajad Sadough, and Imran Shafique Ansari. "Tractable optical channel modeling between UAVs." IEEE Transactions on Vehicular Technology 68.12 (2019): 11543-11550.
7. Dabiri, Mohammad Taghi, Seyed Mohammad Sajad Sadough, and Mohammad Ali Khalighi. "Channel modeling and parameter optimization for hovering UAV-based free-space optical links." IEEE Journal on Selected Areas in Communications 36.9 (2018): 2104-2113.
8. Dabiri, Mohammad Taghi, and Seyed Mohammad Sajad Sadough. "Optimal placement of UAV-assisted free-space optical communication systems with DF relaying." IEEE Communications Letters 24.1 (2019): 155-158.
9. Dabiri, Mohammad Taghi, et al. "UAV-assisted free space optical communication system with amplify-and-forward relaying." IEEE Transactions on Vehicular Technology 70.9 (2021): 8926-8936.
10. Dabiri, Mohammad Taghi, et al. "Modulating retroreflector based free space optical link for UAV-to-ground communications." IEEE Transactions on Wireless Communications 21.10 (2022): 8631-8645.
11. Dabiri, Mohammad Taghi, et al. "How Secure Are UAV-Based FSO Links With Modulating Retroreflectors?." IEEE Wireless Communications Letters (2024).
12. Dabiri, Mohammad Taghi, Himan Savojbolaghchi, and Seyed Mohammad Sajad Sadough. "On the ergodic capacity of ground-to-uav free-space optical communications." 2019 2nd West Asian Colloquium on Optical Wireless Communications (WACOWC). IEEE, 2019.
13. Dabiri, Mohammad Taghi, and Seyed Mohammad Sajad Sadough. "Outage analysis of UAV-based FSO systems over log-normal turbulence channels." 2019 2nd West

Asian Colloquium on Optical Wireless Communications (WACOWC). IEEE, 2019.
14. Wang, Jin-Yuan, et al. "Hovering UAV-based FSO communications: Channel modelling, performance analysis, and parameter optimization." IEEE Journal on Selected Areas in Communications 39.10 (2021): 2946-2959.
15. Gismalla, Mohammed SM, et al. "Performance Analysis of Multi-Hop UAVs Using FSO Communications Under Humidity and Sandstorms Conditions." IEEE Open Journal of the Communications Society (2024).
16. Ortiz, Gerardo G., et al. "Design and development of a robust ATP subsystem for the altair UAV-to-ground lasercomm 2.5-Gbps demonstration." Free-Space Laser Communication Technologies XV. Vol. 4975. SPIE, 2003.
17. Chlestil, Christoph, et al. "Optical wireless on swarm UAVs for high bit rate applications." Proc. IEEE Conf. CSNDSP. 2006.
18. Nallagonda, Vijaya Ratnam, and Prabu Krishnan. "Bit error rate analysis of polarization shift keying based free space optical link over different weather conditions for inter unmanned aerial vehicles communications." Optical and Quantum Electronics 53.9 (2021): 538.
19. Heng, K. H., et al. "Adaptive beam divergence for inter-UAV free space optical communications." 2008 IEEE PhotonicsGlobal@ Singapore. IEEE, 2008.
20. Nallagonda, Vijaya Ratnam, and Prabu Krishnan. "Performance analysis of FSO based inter-UAV communication systems." Optical and Quantum Electronics 53 (2021): 1-20.
21. Moon, Hyung-Joo, et al. "A generalized pointing error model for FSO links with fixed-wing UAVs for 6G: Analysis and trajectory optimization." IEEE Transactions on Wireless Communications (2025).
22. Wu, Yan, et al. "Performance analysis of UAV-assisted hybrid FSO/RF communication systems under various weather conditions." Sensors 23.17 (2023): 7638.
23. Petkovic, Milica, Aleksandra Cvetkovic, and Milan Narandzic. "Outage probability analysis of RF / FSO-VLC communication relaying system." 2018 11th International Symposium on Communication Systems, Networks and Digital Signal Processing (CSNDSP). IEEE, 2018.
24. Pradhan, Jayashree, Vinod Kiran Kappala, and Santos Kumar Das. "Performance analysis of a Li-Fi system under ambient light conditions." 2020 National Conference on Communications (NCC). IEEE, 2020.
25. Ali, Mohammad Furqan, et al. "Dual-hop mixed FSO-VLC underwater wireless communication link." IEEE Transactions on Network and Service Management 19.3 (2022): 3105-3120.
26. Komine, Toshihiko, and Masao Nakagawa. "Fundamental analysis for visible-light communication system using LED lights." IEEE transactions on Consumer Electronics 50.1 (2004): 100-107.
27. Gupta, Akash, et al. "Cascaded FSO-VLC communication system." IEEE Wireless Communications Letters 6.6 (2017): 810-813.
28. Sharma, Harsh, et al. "An approach for secure communication using LiFi technology with laser in border areas." 2024 International conference on advances in computing, communication and applied informatics (ACCAI). IEEE, 2024.
29. Basnayaka, Dushyantha A., and Harald Haas. "Design and analysis of a hybrid radio frequency and visible light communication system." IEEE Transactions on Communications 65.10 (2017): 4334-4347.
30. Yin, Liang, et al. "Performance evaluation of non-orthogonal multiple access in visible light communication." IEEE Transactions on Communications 64.12 (2016): 5162-5175.
31. de Souza Lopes, Celso Henrique, et al. "Implementation of HetNet architectures based on FSO, VLC, RoF, and photonics-based RF generation toward 6G applications." Journal of Optical Communications and Networking 16.10 (2024): 1070-1081.